BMC Medical Imaging

RESEARCH Open Access

Application research on the diagnosis of classic trigeminal neuralgia based on VB-Net technology and radiomics

Lei Pan[1†], Xuechun Wang[2†], Xiuhong Ge[1], Haiqi Ye[1], Xiaofen Zhu[1], Qi Feng[1], Haibin Wang[1], Feng Shi[2*] and Zhongxiang Ding[1*]

Abstract

Background This study aims to utilize the deep learning method of VB-Net to locate and segment the trigeminal nerve, and employ radiomics methods to distinguish between CTN patients and healthy individuals.

Methods A total of 165 CTN patients and 175 healthy controls, matched for gender and age, were recruited. All subjects underwent magnetic resonance scans. VB-Net was used to locate and segment the bilateral trigeminal nerve of all subjects, followed by the application of radiomics methods for feature extraction, dimensionality reduction, feature selection, model construction, and model evaluation.

Results On the test set for trigeminal nerve segmentation, our segmentation parameters are as follows: the mean Dice Similarity Coefficient (mDCS) is 0.74, the Average Symmetric Surface Distance (ASSD) is 0.64 mm, and the Hausdorff Distance (HD) is 3.34 mm, which are within the acceptable range. Analysis of CTN patients and healthy controls identified 12 features with larger weights, and there was a statistically significant difference in Rad_score between the two groups ($p < 0.05$). The Area Under the Curve (AUC) values for the three models (Gradient Boosting Decision Tree, Gaussian Process, and Random Forest) are 0.90, 0.87, and 0.86, respectively. After testing with DeLong and McNemar methods, these three models all exhibit good performance in distinguishing CTN from normal individuals.

Conclusions Radiomics can aid in the clinical diagnosis of CTN, and it is a more objective approach. It serves as a reliable neurobiological indicator for the clinical diagnosis of CTN and the assessment of changes in the trigeminal nerve in patients with CTN.

Keywords Classic trigeminal neuralgia, Deep learning, Radiomics, Neuroimaging

[†]Lei Pan and Xuechun Wang contributed equally to this work.

*Correspondence:
Feng Shi
feng.shi@uii-ai.com
Zhongxiang Ding
hangzhoudzx73@126.com
[1]Department of Radiology, Affiliated Hangzhou First People's Hospital, School of Medicine, Westlake University, Hangzhou 310000, Zhejiang, China
[2]Department of Research and Development, Shanghai United Imaging Intelligence Co., Ltd, 701 Yunjin Road, Shanghai 200030, China

Introduction

Trigeminal neuralgia (TN) is a debilitating chronic facial pain disease, which is typically characterized by transient, paroxysmal, and electric shock-like unilateral pain attacks, mostly on the right side [1]. It is called the most unbearable pain for human beings. The pain is distributed in one or more branches of the trigeminal nerve, mainly the second branch (maxillary branch) or the third branch (mandibular branch). The incidence of TN is higher in women than in men and increases with age [2–4]. It is estimated that the annual incidence of TN is approximately 4 to 13 per 100,000 people [5]. The onset of TN can be caused by some daily actions, such as talking, eating, brushing teeth, washing face, etc., or it can occur without any inducement [6]. TN patients often feel nervous or fearful of the pain that may come at any time. If they endure this huge pressure for a long time, they may develop anxiety and depression, leading to a continuous decline in their quality of life. Therefore, it is of great clinical significance to distinguish TN patients from normal people earlier and treat patients in a timely manner.

According to the International Classification of Headache Disorders (ICHD-3) [7], TN is divided into three subtypes: classic trigeminal neuralgia (CTN), secondary TN and idiopathic TN. Neurovascular compression (NVC) is considered to be the main cause of CTN, and NVC can be treated by microvascular decompression (MVD) surgery [8], although most CTN patients with NVC experience pain after MVD. are relieved, but NVC can also be observed in asymptomatic people [9, 10]. Studies have shown that 25–49% of healthy individuals and 14–39% of cadavers also have this anatomical variation [11]. Therefore, NVC is only one of the causes of CTN.

In 2012, Dutch scholar Lambin and others first proposed the concept of radiomics in the European Journal of Cancer [12]. Radiomics is a high-throughput data mining method that can use computer technology to fully mine the information hidden in images, and then combine this hidden information to analyze different clinical phenotypes of the disease. In recent years, there have been an increasing number of studies related to radiomics and TN. Zhong et al. [13] used a linear support vector machine algorithm to distinguish inter-regional normalized streamline counts between TN and HC. The algorithm successfully distinguished TN and HC with an accuracy of 88%. Willsey et al. [14] used pontine radial diffusivity (RD) and symptom duration (DS) classifiers to accurately predict the recurrence of trigeminal neuralgia after microvascular decompression, and the accuracy of the 2 classifiers in predicting pain-free remission and eventual recurrence It was 85%, the sensitivity was 83%, and the specificity was 86%. Chen et al. [15] used a Gaussian process classifier to discover changes in the bilateral trigeminal nerve, distinguishing them from controls with an accuracy of 80%, and could distinguish the affected side from the unaffected side with an accuracy of 75%. affected side. Ge et al. [16] of this research team used machine learning (ML) to explore the risk factors of unilateral CTN or ITN-nvc (UC-ITN) with bilateral NVC, and found that in addition to NVC, the texture characteristics of the cisternal segment of the trigeminal nerve and responsible vessel (Ofv) are also risk factors for UC-ITN. It can be seen that radiomics plays a positive role in the prediction of diagnosis and treatment and the exploration of the cause of CTN.

This study pioneered the utilization of VB-Net's deep learning method to accurately locate and segment the trigeminal nerve. Subsequently, a classification model was constructed through radiomics to distinguish between CTN patients and healthy individuals, ultimately aiding in the clinical diagnosis and treatment of CTN.

Materials and methods

Image acquisition

Clinical data

This study was approved by the Ethics Committee of Hangzhou First People's Hospital Affiliated to Zhejiang University School of Medicine (IRB# NO.202107002). Clinical and imaging data were collected from CTN patients who were treated at the hospital from April 2021 to April 2022 and underwent MRI scans. The inclusion criteria were: (1) Meeting the diagnostic criteria for classic TN according to the International Classification of Headache Disorders (ICHD-3) [7]; (2) Completion of a comprehensive MRI scan, including at least 3D volume interpolation body examination (3D-VIBE) and 3D short-term inversion recovery sequence (3D-STIR); (3) Being right-handed. The exclusion criteria were: (1) Having undergone TN-related surgical treatment; (2) Having a clear history of neurological diseases such as brain trauma, cerebral hemorrhage, or brain tumors; (3) The presence of heavy image artifacts or poor quality affecting the final evaluation; (4) Symptoms occurring on both sides. Ultimately, 165 patients were included in this study (see Fig. 1 for details). Healthy individuals matching the patient group in gender and age were also included. The inclusion criteria for healthy controls were: (1) No previous history of neurological, psychiatric, or pain diseases; (2) No previous history of major central nervous system surgery; (3) No contraindications to MRI scanning. Ultimately, 175 healthy controls were included in this study. There was no statistically significant difference in gender and age between the patient group and the healthy control group ($p>0.05$) (see Table 1 for details).

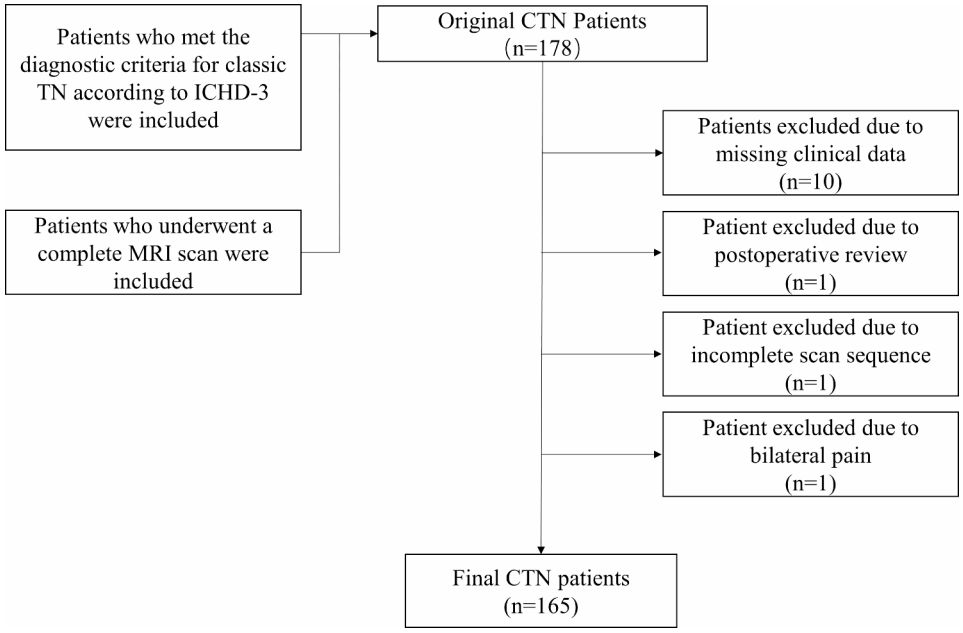

Fig. 1 Inclusion and exclusion criteria flow chart of CTN

Table 1 Clinical data of CTN patients and healthy controls

	CTN patients	Healthy controls	χ^2/t	*P*
Number	165 (48.5)	175 (51.5)	/	/
Sex(M/F)	58/107	58/117	0.152	0.696[a]
Age	55.6 ± 13.9	55.2 ± 12.3	0.293	0.770[b]

CTN: classical trigeminal neuralgia; P[a]: Chi-square test; P[b]: independent-sample t test

Inspection method

All scans were performed using a 3.0T MRI scanner (Discovery MR Verio, Siemens, Germany) equipped with an 8-channel head coil, with participants positioned in the supine position. Foam pads and headphones were utilized to minimize head movement and reduce scanner noise. The acquisition protocol comprised the following:

(1) 3D-VIBE sequence: repetition time of 10ms, echo time of 3.69ms, flip angle of 12°, field of view of 220×220, voxels of 0.8×0.8×0.8, slice thickness of 0.8 mm, encompassing 60 axial slices.

(2) 3D-STIR sequence: repetition time of 3800ms, echo time of 194ms, flip angle of 12°, field of view of 230×230, voxels of 0.9×0.9×0.9, slice thickness of 0.9 mm, encompassing 64 axial slices.

All scanned images were transferred to a research platform, the uAI research portal (https://www.uii-ai.com/en/uai/scientific-research) [17].

Image segmentation

The two-stage framework for the root entry zone of trigeminal nerves segmentation

The proposed framework employs a two-stage segmentation strategy. First, a VB-Net [18, 19] is used to segment the pons region on the brain images. Since the root entry zones of trigeminal nerve are too small to be segmented directly and which are adjacent to the pons, we segment pons at the coarse level for localization of the roots of nerves. Then, we calculate the bounding box of pons and expanded 5 pixels on the three axis as the input of the second stage segmentation network. VB-Net is also used to segment the root zones of trigeminal nerve at the second stage, and the segmentation results are mapped bask to original image. Figure 2a shows the overview of the proposed architecture. The two-stage network strategy not only filters out the background and focus on the target area in the subsequent processing steps, but also greatly reduce the image size input to the second-stage network which speeds up the training and inferring of the network.

The VB-Net is an improved network which combines V-Net [20] with bottleneck structures to reduce the parameter and speed up the convergence of network [18, 19]. As shown in Fig. 2b, the VB-Net consists of one input block, four down block, four up block, and one out block. The encoding path consists of an input block and four down block which extracts high-level context information through 3D convolution layers. The decoding path (four up block and one output block) integrates high-level features and local fine-grained image features by skip connections. Specifically, the input block is a convolution module which includes a convolution module (kernel size: 3×3×3, stride size: 1×1×1) and followed by a BN layer and a ReLU layer; the output block includes a convolution module, a global average pooling layer and a Softmax layer. In addition, the down/up block consists

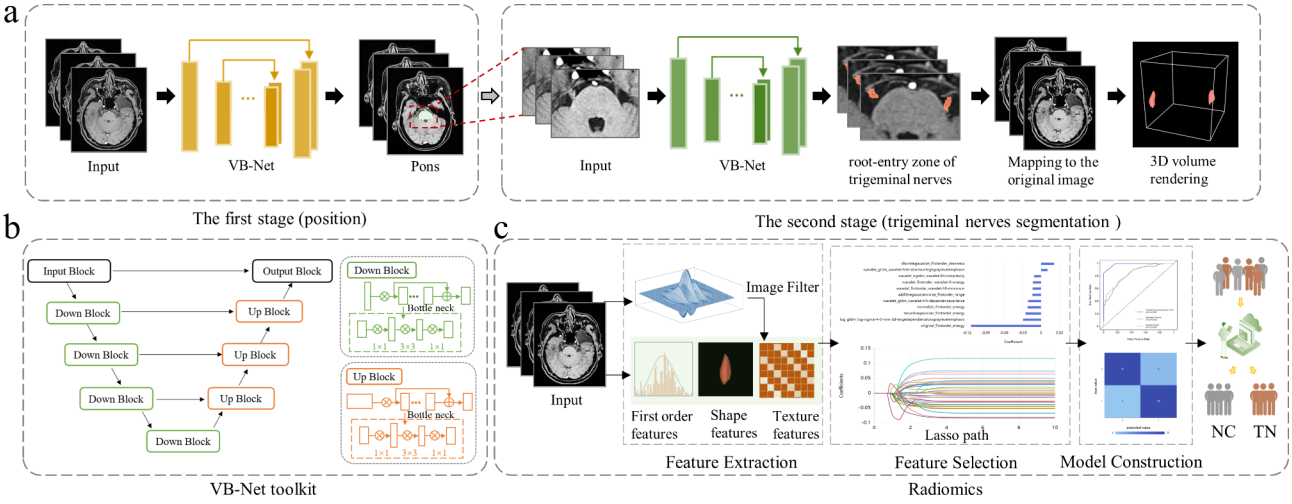

Fig. 2 The workflow for identifying patients with TN. **a**. The two-stage framework for the root entry zone of trigeminal nerves segmentation. **b**. The architecture of VB-Net toolkit. **c**. The process of radiomics analysis

of one convolution/ de-convolution module with several bottleneck module. In the encoding path, the number of bottleneck structure are set as 1, 2, 3, 3 in turn, and the decoding path is 3, 3, 2, 1, respectively.

Data preprocessing and augmentation

In the first stage, we resample the image to [1, 1, 1] mm^3 , and randomly crop the patch of [96, 96, 96] $pixel^3$ on the images to train the network. In the second stage, the images are resampled to [0.8, 0.8, 0.8] mm^3, and the input patch are reshaped to [64, 64, 64] $pixel^3$ (padding 0). Before these patches fed into network, we use adaptive normalization algorithm on these patches. To be specific, the patch is normalized with Z-score (the mean and standard deviation of each image calculated in the intensity range of 0.1 to 99.9), and then the intensity is clipped to [-1, 1]. Additionally, data augmentation is applied to improve the generalization of network, which includes random shifting (0∼5 mm), slight scaling (0.9∼1.1), and rotation (-10° ∼ +10°) on the cropped images.

Loss function

We combine DSC loss and Focal loss to optimize the network, and the weight for each loss is 0.5. The loss function (L_{hybrid}) for segmentation is defined as:

$$L_{dice} = 1 - \frac{2 \times \ V_P \ \times \ V_L}{V_P + \ V_L}$$

$$L_{focal} = -\alpha\,(1 - V_p)^{\gamma} \times V_L \log V_p - (1 - \alpha\,)V_p^{\gamma}\,(1 - V_L)\log(1 - V_p)$$

$$L_{hybrid} = 0.5{*}L_{dice} + 0.5{*}L_{focal}$$

whereV_L and $V_P$denote the ground truth and the predicted segmentation result.

Implement details

The proposed framework was implemented using Python and PyTorch 1.7.0. Kaiming initialization was used to initialize kernel weights. The Adam optimizer was used with a learning rate of 1e-4, β1 of 0.9, β2 of 0.999 and weight decay setting as 0. We performed 5000 epochs to train the network, and the batch size was set to 32. All experiments were performed on an NVIDIA GeForce RTX 2080 Ti graphic card with 12G memory.

Radiomics

Using the uAI research portal (uRP) software [17], radiomics feature analysis was performed on the subject's bilateral trigeminal nerve images. The specific steps are as follows:

① Feature extraction: This step is carried out based on the original image and the region of interest (ROI) obtained from the deep learning model. The features are categorized into three groups: shape features, texture features, and grayscale statistical features. Multiple filtering processes are applied to the image during this stage.

② Feature selection: Dimension reduction methods employed include variance threshold (0.8), K best (100), and least absolute shrinkage and selection operator regression (LASSO). LASSO is utilized to select the most predictive feature subset and evaluate the corresponding coefficient.

③ Model construction: The ratio of the training set and test set is randomly set to 0.8 and 0.2, respectively. The selected features are weighted by their coefficients, and the resulting value is used as a measure called Rad_score. This Rad_score is then compared between the training set and the test set.

④ Model evaluation: The difference is initially quantified using the area under the curve (AUC) of the receiver

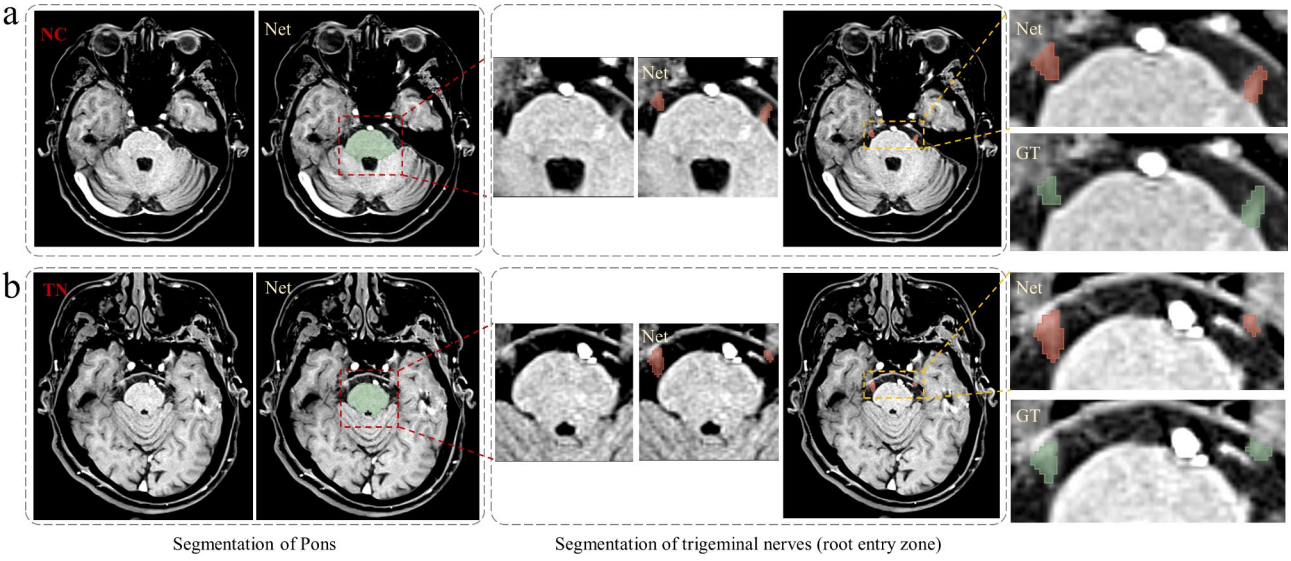

Fig. 3 Two examples showing the performance of trigeminal nerves (root entry zone) segmentation. **a**. segmentation flow of NC. **b**. segmentation flow of TN

operating characteristic (ROC) curve. Subsequently, a calibration curve is used to estimate the agreement between the predictive model and actual outcomes. A confusion matrix is employed to evaluate model accuracy. Finally, the net clinical benefit of the predictive model is visualized through a decision curve. (See Fig. 2c for details.)

Statistical methods

SPSS 26.0 and R (Version 4.0.2) were utilized for statistical analysis. Clinical and MRI morphological features were assessed using the chi-square test for nominal variables and the Wilcoxon test for continuous variables. The independent samples t-test was employed for group comparisons. The receiver operating characteristic (ROC) curve analysis within the machine learning module was used to evaluate model performance, allowing us to obtain model evaluation indicators such as the area under the ROC curve (AUC). Decision curve analysis was applied to assess the net benefit of the models at different diagnostic thresholds. Lastly, the DeLong and McNemar tests were utilized for model comparison. A p-value <0.05 was considered statistically significant for all analyses.

Results

The performance of trigeminal nerves (root entry zone) segmentation

A total of 179 images are divided into training (123), validation (20), and testing (36) sets. We optimized the configuration of network and tested the best training epoch on the validation set. Figure 3 demonstrates the segmentation flow of two examples (Fig. 3a: NC; Fig. 3b: TN), and TN patients show obvious vascular compression on the right root zone of trigeminal nerve. In Fig. 3, firstly, pons is segmented on the whole images as the first step, and then the bounding box cropped based on the pons segmentation as the input to the second stage. The second VB-Net segments the roots of trigeminal nerve and mapping to the original image. Figure 3 shows decent agreement between the ground truth and network result. On the testing set, we achieved a mean Dice Similarity Cofficient(mDCS) [21] of 0.74±0.08, Average Symmetric Surface Distance(ASSD) [22] of 0.65±1.36 mm, and Hausdorff Distance(HD) [23] of 2.35±3.32 mm (See Table 2 for details). There are few studies directly segmenting the root entry zone of the trigeminal nerve, though it is clinically significant for trigeminal neuralgia patients. Due to variations in imaging modalities, training data, and segmented regions, direct comparisons

Table 2 Network parameter comparison experiment

model	Dice	ASSD(mm)	HD(mm)
U-Net	0.42±0.20	6.42±3.47	11.82±5.30
VB-Net	0.53±0.19	5.05±4.07	11.21±8.70
Two stage VB-Net (no expand)	0.62±0.16	1.64±2.74	6.04±6.10
Two stage VB-Net (expand 1 pixel)	0.62±0.15	1.58±2.69	5.93±6.11
Two stage VB-Net (expand 2 pixel)	0.64±0.17	1.55±2.70	5.43±6.21
Two stage VB-Net (expand 3 pixel)	0.68±0.11	1.18±2.04	4.59±7.20
Two stage VB-Net (expand 4 pixel)	0.70±0.14	1.11±1.91	3.61±4.52
Two stage VB-Net (expand 5 pixel)	0.74±0.08	0.65±1.36	2.35±3.32

ASSD: Average Symmetric Surface Distance; HD: Hausdorff Distance

are challenging. Our manuscript reports a Dice score of 0.74 for segmenting the trigeminal nerve root entry zone, comparable to existing literature.

Radiology analysis

A total of 2264 features were extracted from each region of interest (ROI). After applying dimension reduction techniques such as variance threshold (0.8), K best (100), and LASSO, 12 features with significant weights were selected. These features included Variance, Skewness, Short Run High Gray Level Emphasis (SRHGLE), Complexity, Wavelet Energy, Minimum, Range, Dependence Variance, Normalize Energy, Recursive Gaussian Energy, Large Dependence Low Gray Level Emphasis, and Original Energy. The Rad_score indicated a statistical difference between the trigeminal neuralgia (TN) patient group and the healthy control group ($p<0.05$). The area under the curve (AUC) values for the training set and the test set were consistent, indicating a good fit for the model. The AUCs of the three models—Gradient Boosting Decision Tree, Gaussian Process, and Random Forest—were 0.90, 0.87, and 0.86, respectively. The calibration curves for both the training and test sets demonstrated the high accuracy of the model. The confusion matrix further confirmed the model's high accuracy. The decision curve analysis proved that the model could achieve higher clinical benefit. Overall, all three models performed well in distinguishing TN patients from healthy individuals. (See Fig. 4; Tables 3 and 4 for details.)

Discussion

In this study, we utilized both the positioning and segmentation technology of deep learning and the classification function of radiomics to identify patients with trigeminal neuralgia (CTN) and healthy individuals. The research results revealed that Variance, Skewness, Short Run High Gray Level Emphasis (SRHGLE), Complexity, Wavelet Energy, Minimum, Range, Dependence Variance, Normalize Energy, Recursive Gaussian Energy, Large Dependence Low Gray Level Emphasis, and Original Energy had larger weights. Most of the features included in the prediction models were based on grayscale statistics, which quantitatively describe the distribution of voxel intensities in an image through common and basic measures. This may be because the trigeminal nerve is displaced or deformed, or even undergoes demyelination changes, which subsequently lead to alterations in the aforementioned characteristics. The comparisons of the area under the curve (AUC) values for different models were performed using the DeLong test, while the assessments of sensitivity, specificity, and accuracy were conducted using the McNemar test. The results from Table 4 indicate that there were no significant evaluation differences between any two of the three models, and all of them demonstrated good classification performance.

VB-Net exhibits superior segmentation performance for the trigeminal nerve. Previous research [24] introduced a lightweight and rapid semantic segmentation network for microvascular decompression (MVD) scenes, termed MVD-Net, which achieves a commendable balance between segmentation accuracy and speed. The specific methodology involves designing a Light Asymmetric Bottleneck (LAB) module within the encoder to encode contextual features, and incorporating a Feature Fusion Module (FFM) in the decoder to effectively combine high-level semantic features with underlying spatial details. However, the proposed network lacks a pre-trained model and specificity for application in real-world scenarios. In this study, a total of 179 images were allocated to the segmentation network, divided into training sets (123), validation sets (20), and test sets (36). A two-stage segmentation strategy was employed, fully acknowledging that the root entry area of the trigeminal nerve is too small for direct division. The two-stage network adopts a "localize first, then segment" approach: the brain segmentation network serves as the localization network, utilizing the pons area at the entry of the trigeminal nerve root for localization. Based on the localization network, VB-Net is used to perform accurate segmentation of the trigeminal nerve near the pons area of the image at its original resolution. Additionally, the two-stage network strategy not only filters out the background and focuses on the target area in subsequent processing steps but also significantly reduces the size of the image input to the second-stage network, thereby accelerating the training and inference of the network.

Anatomical changes in the trigeminal nerve in CTN patients can be detected through radiomics analysis following VB-Net segmentation. Similarly, Mulford et al. [25] employed a U-net deep learning method for segmenting and analyzing the trigeminal nerve, extracting 216 features from each nerve. They trained a neural network to distinguish between TN-affected nerves, achieving an accuracy of 78%, an AUC of 0.83, a sensitivity of 0.82, and a specificity of 0.76 in a study involving 134 patients. The three models used in this study—gradient descent tree, Gaussian process, and random forest—all exhibited good predictive performance in distinguishing TN from normal individuals. The AUCs for the test set were 0.861, 0.874, and 0.855, respectively. Other studies have utilized whole-brain features extracted from MRI to identify changes in TN patients. Mo et al. [26] compared cortical thickness, surface area, and neocortical myelin levels between TN patients and healthy subjects (43:43) using MRI. The results revealed reduced cortical indices in the anterior cingulate cortex (ACC), middle cingulate cortex (MCC), and posterior cingulate cortex (PCC) in

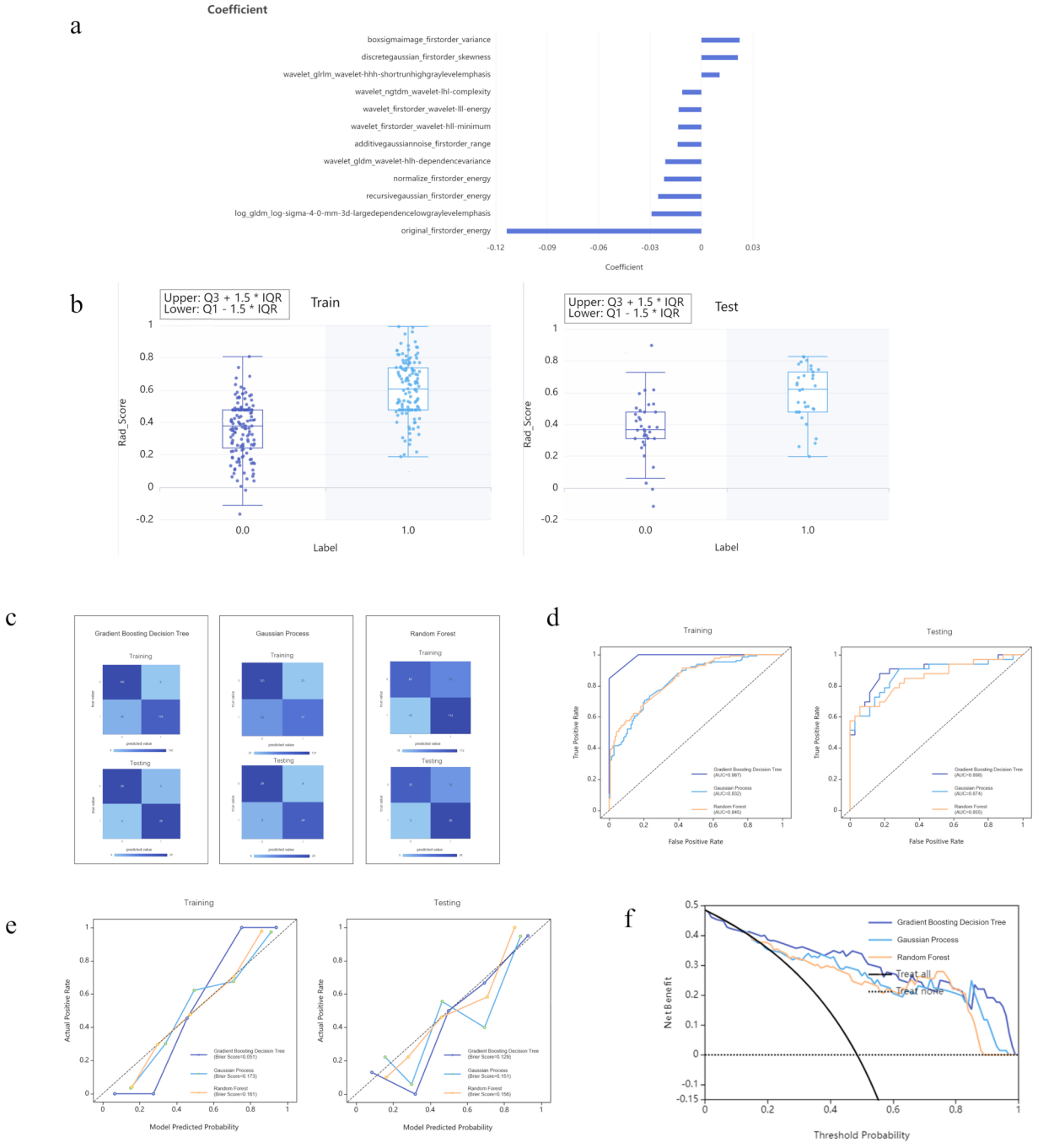

Fig. 4 Feature selection, model construction and evaluation. **a**. Selection of features with greater weight between the two groups. **b**. Rad_score of the training and testing sets. **c**. Confusion matrix. **d**. ROC of training and testing sets. **e**. Calibration curves of training and testing sets. **f**. Decision curve

patients with TN, indicating that morphological changes at the whole-brain level successfully enabled automated TN diagnosis with high specificity. Hung et al. [27] employed a data-driven approach that combined retrospective structural neuroimaging data and support vector machine-based machine learning to produce robust multivariate prediction models of pain relief following Gamma Knife radiosurgery for trigeminal neuralgia. They found that the best predictor for the regional surface area model and the regional cortical thickness model was the contralateral superior frontal gyrus and contralateral isthmus cingulate gyrus, respectively. Compared to such

Table 3 Parameters of the three models

preprocessor	classification	group	AUC	sensitivity	specificity	accuracy	precison
L1_normalization	GBDT	Train cohort	0.983(0.969–0.996)	0.866	0.958	0.914	0.951
		Validation cohort	0.861(0.76–0.961)	0.750	0.871	0.814	0.840
	GaussianProcess	Train cohort	0.832(0.784–0.879)	0.592	0.852	0.728	0.786
		Validation cohort	0.874(0.786–0.961)	0.727	0.829	0.779	0.8
	RadomForest	Train cohort	0.845(0.801–0.889)	0.862	0.599	0.724	0.663
		Validation cohort	0.855(0.764–0.947)	0.848	0.657	0.75	0.7

GBDT: Gradient Boosting Decision Tree

Table 4 The *P* value of validation cohort of Delong and McNemar

model comparison	AUC	sensitivity	specificity	accuracy
GP VS GBDT	0.202	0.062	1.000	1.000
GP VS RF	0.462	1.000	1.000	1.000
GBDT VS RF	0.060	0.031	1.000	1.000

GP: Gaussian Process; GBDT: Gradient Boosting Decision Tree; RF: Random Forest

studies, this study extracted the radiomics features of the trigeminal nerve itself, which is a more direct and reliable approach than using whole-brain features.

Currently, research both domestically and internationally primarily concentrates on imaging studies of neurovascular conflicts, which are identified by radiologists or surgeons during surgical procedures [28–30]. These studies seldom involve images of the trigeminal nerve obtained solely through MRI scanning. There is a lack of intelligent and automated diagnosis methods, especially in screening diagnosis. The novelty of this study lies in the utilization of the VB-Net deep learning method to accurately locate and segment the trigeminal nerve, and the establishment of a diagnostic model through radiomics. This approach offers a novel idea for efficient clinical diagnosis of CTN. Furthermore, this study directly analyzes the trigeminal nerve itself, whereas most current CTN imaging studies both domestically and internationally still rely on whole-brain analysis.

The limitation of this study is that it did not conduct a comparative analysis with other craniofacial pain diseases. Additionally, the sample size at this stage is still relatively small, and it is a single-center study. In the future, we can continue to broaden the scope of research diseases and increase the scale of the study to make the data and conclusions more compelling. We can also enrich the content of longitudinal research and integrate information following MVD surgery to predict and evaluate patient outcomes.

Conclusion

In summary, VB-Net demonstrates the ability to accurately locate and segment the trigeminal nerve, and radiomics can assist in the clinical diagnosis of CTN. CTN is a chronic pain disorder that significantly impacts the daily lives of patients, yet its specific pathogenesis remains unclear. It is currently hypothesized that it may be associated with abnormal structure and function of the trigeminal nerve, resulting from a combination of congenital and secondary factors. In the early stages, patients may not take CTN seriously or it may be misdiagnosed as other pain disorders, leading to delayed treatment. Traditional clinical diagnosis methods are subject to considerable subjectivity and limitations. However, the rapid advancements in neuroimaging in recent years have provided more objective and sensitive neurobiological indicators for the diagnosis of CTN, which is of great significance for early diagnosis and treatment.

Abbreviations

ASSD	Average Symmetric Surface Distance
AUC	Area under the curve
CTN	Classic Trigeminal Neuralgia
DCS	Dice Similarity Cofficient
GBDT	Gradient Boosting Decision Tree
GP	Gaussian Process
HD	Hausdorff Distance
LASSO	Least absolute shrinkage and selection operator regression
ML	Machine learning
MRI	Magnetic resonance imaging
MVD	Microvascular decompression
NVC	Neurovascular compression
RF	Random Forest
ROC	Receiver operating characteristic
ROI	Region of interest
SRHGLE	Short Run High Gray Level Emphasis

Acknowledgements

Not applicable.

Author contributions

LP, HY, XZ and XG collected relevant data, FS and ZD analyzed and interpreted the patient data regarding the parametric features. LP and XW wrote the main manuscript and prepared Figs. 1, 2, 3 and 4. XG, ZD, HW and QF provided the funding help. All authors read and approved the final manuscript.

Funding

This study is supported by Hangzhou Agriculture and Social Development Scientific Research Guidance Project (20211231Y022), National Natural Science Foundation of China (81871337), Zhejiang Medical and Health Research Project (2021RC102), Zhejiang Provincial Medical and Health Technology Project (2024KY1313).

Data availability

Data and material in the study are available from the corresponding author on reasonable request.

Declarations

Ethics approval and consent to participate

This study was approved by Ethics Committee of Hangzhou First People's Hospital, and informed consent was waived for patients in this retrospective study.

Consent for publication

Not applicable.

Competing interests

The authors declare no competing interests.

Received: 14 January 2024 / Accepted: 9 September 2024
Published online: 16 September 2024

References

1. Tohyama S, Walker MR, Zhang JY, Cheng JC, Hodaie M. Brainstem trigeminal fiber microstructural abnormalities are associated with treatment response across subtypes of trigeminal neuralgia. Pain. 2021;162(6):1790–9. https://doi.org/10.1097/j.pain.0000000000002164
2. Jones MR, Urits I, Ehrhardt KP, et al. A comprehensive review of trigeminal neuralgia. Curr Pain Headache Rep. 2019;23(10):74. https://doi.org/10.1007/s11916-019-0810-0
3. Cruccu G, Di Stefano G, Truini A. Trigeminal Neuralgia. N Engl J Med. 2020;383(8):754–62. https://doi.org/10.1056/NEJMra1914484
4. Leal PR, Hermier M, Froment JC, Souza MA, Cristino-Filho G, Sindou M. Preoperative demonstration of the neurovascular compression characteristics with special emphasis on the degree of compression, using high-resolution magnetic resonance imaging: a prospective study, with comparison to surgical findings, in 100 consecutive patients who underwent microvascular decompression for trigeminal neuralgia. Acta Neurochir (Wien). 2010;152(5):817–25. https://doi.org/10.1007/s00701-009-0588-7
5. Gambeta E, Chichorro JG, Zamponi GW. Trigeminal neuralgia: an overview from pathophysiology to pharmacological treatments. Mol Pain. 2020;16:1744806920901890. https://doi.org/10.1177/1744806920901890
6. Sessle BJ. Mechanisms of oral somatosensory and motor functions and their clinical correlates. J Oral Rehabil. 2006;33(4):243–61. https://doi.org/10.1111/j.1365-2842.2006.01623.x
7. Headache Classification Committee of the International Headache Society (IHS). The international classification of headache disorders, 3rd edition. Cephalalgia. 2018;38(1):1–211. https://doi.org/10.1177/0333102417738202
8. Cruccu G. Trigeminal neuralgia. Continuum (Minneap Minn). 2017;23(2, Selected Topics in Outpatient Neurology):396–420. https://doi.org/10.1212/CON.0000000000000451
9. Zakrzewska JM, Akram H. Neurosurgical interventions for the treatment of classical trigeminal neuralgia. Cochrane Database Syst Rev. 2011;2011(9):CD007312. https://doi.org/10.1002/14651858.CD007312.pub2
10. Ferguson GG, Brett DC, Peerless SJ, Barr HW, Girvin JP. Trigeminal neuralgia: a comparison of the results of percutaneous rhizotomy and microvascular decompression. Can J Neurol Sci. 1981;8(3):207–14. https://doi.org/10.1017/s0317167100043225
11. Wang Y, Yang Q, Cao D, et al. Correlation between nerve atrophy, brain grey matter volume and pain severity in patients with primary trigeminal neuralgia. Cephalalgia. 2019;39(4):515–25. https://doi.org/10.1177/0333102418793643
12. Lambin P, Rios-Velazquez E, Leijenaar R, et al. Radiomics: extracting more information from medical images using advanced feature analysis. Eur J Cancer. 2012;48(4):441–6. https://doi.org/10.1016/j.ejca.2011.11.036
13. Zhong J, Chen DQ, Hung PS, et al. Multivariate pattern classification of brain white matter connectivity predicts classic trigeminal neuralgia. Pain. 2018;159(10):2076–87. https://doi.org/10.1097/j.pain.0000000000001312
14. Willsey MS, Mossner JM, Chestek CA, Sagher O, Patil PG. Classifier using Pontine radial diffusivity and symptom duration accurately predicts recurrence of trigeminal neuralgia after microvascular decompression: a pilot study and algorithm description. Neurosurgery. 2021;89(5):777–83. https://doi.org/10.1093/neuros/nyab292
15. Chen DQ, Zhong J, Chu PPW, Fei Li CM, Hodaie M. Trigeminal neuralgia diffusivities using gaussian process classification and merged group tractography. Pain. 2021;162(2):361–71. https://doi.org/10.1097/j.pain.0000000000002023
16. Ge X, Wang L, Pan L, et al. Risk factors for unilateral trigeminal neuralgia based on machine learning. Front Neurol. 2022;13:862973. https://doi.org/10.3389/fneur.2022.862973
17. Wu J, Xia Y, Wang X, et al. uRP: an integrated research platform for one-stop analysis of medical images. Front Radiol. 2023;3:1153784. https://doi.org/10.3389/fradi.2023.1153784
18. Han M, Yao G, Zhang W et al. Segmentation of CT thoracic organs by multi-resolution VB-nets. SegTHOR@ISBI. 2019.
19. Shi F, Hu W, Wu J, et al. Deep learning empowered volume delineation of whole-body organs-at-risk for accelerated radiotherapy. Nat Commun. 2022;13(1):6566. https://doi.org/10.1038/s41467-022-34257-x. Published 2022 Nov 2.
20. Milletari F, Navab N, Ahmadi SA, Ahmadi. V-net: Fully convolutional neural networks for volumetric medical image segmentation, in 2016 Fourth International Conference on 3D Vision (3DV), 2016, pp. 565–571: IEEE. https://doi.org/10.1109/3DV.2016.79
21. Gerig G, Jomier M, Chakos M. Valmet: a new validation tool for assessing and improving 3D object segmentation. Int Conf Med Image Comput Computer-assisted Intervention SpringerBerlin Heidelberg. 2001. https://doi.org/10.1007/3-540-45468-3_62
22. Taha AA, Hanbury A. Metrics for evaluating 3D medical image segmentation: analysis, selection, and tool. BMC Med Imaging. 2015;15:29. Published 2015 Aug 12. https://doi.org/10.1186/s12880-015-0068-x
23. Ye S, Ye J. Dice similarity measure between single valued neutrosophic multisets and its application in medical diagnosis. Neutrosophic Sets Syst. 2014;6(1):9–9. https://doi.org/10.5281/zenodo.22448
24. Bai R, Liu X, Jiang S, Sun H. Deep learning based real-time semantic segmentation of cerebral vessels and cranial nerves in microvascular decompression scenes. Cells. 2022;11(11):1830. https://doi.org/10.3390/cells11111830
25. Mulford KL, Moen SL, Grande AW, Nixdorf DR, Van de Moortele PF. Identifying symptomatic trigeminal nerves from MRI in a cohort of trigeminal neuralgia patients using radiomics. Neuroradiology. 2022;64(3):603–9. https://doi.org/10.1007/s00234-022-02900-5
26. Mo J, Zhang J, Hu W, Luo F, Zhang K. Whole-brain morphological alterations associated with trigeminal neuralgia. J Headache Pain. 2021;22(1):95. https://doi.org/10.1186/s10194-021-01308-5
27. Hung PS, Noorani A, Zhang JY, et al. Regional brain morphology predicts pain relief in trigeminal neuralgia. Neuroimage Clin. 2021;31:102706. https://doi.org/10.1016/j.nicl.2021.102706
28. Brînzeu A, Drogba L, Sindou M. Reliability of MRI for predicting characteristics of neurovascular conflicts in trigeminal neuralgia: implications for surgical decision making. J Neurosurg. 2018:1–11. https://doi.org/10.3171/2017.8.JNS171222
29. Hughes MA, Jani RH, Fakhran S, et al. Significance of degree of neurovascular compression in surgery for trigeminal neuralgia. J Neurosurg. 2019:1–6. https://doi.org/10.3171/2019.3.JNS183174
30. Herta J, Schmied T, Loidl TB, et al. Microvascular decompression in trigeminal neuralgia: predictors of pain relief, complication avoidance, and lessons learned. Acta Neurochir (Wien). 2021;163(12):3321–36. https://doi.org/10.1007/s00701-021-05028-2

Publisher's note